AGU PUBLICATIONS

JGR

Journal of Geophysical Research: Solid Earth

RESEARCH ARTICLE
10.1002/2013JB010554

Key Points:
- Flows of fine particles on horizontal rough substrate can be autofluidized
- Autofluidization is due to air escape from the substrate interstices
- Autofluidization is expected to cause long runout of pyroclastic flows

Supporting Information:
- Readme
- Movie S1
- Movie S2
- Movie S3
- Movie S4

Correspondence to:
C. Chedeville,
c.chedeville@opgc.univ-bpclermont.fr

Citation:
Chedeville, C., and O. Roche (2014), Autofluidization of pyroclastic flows propagating on rough substrates as shown by laboratory experiments, *J. Geophys. Res. Solid Earth*, *119*, 1764–1776, doi:10.1002/2013JB010554.

Received 24 JUL 2013
Accepted 21 FEB 2014
Accepted article online 19 MAR 2014
Published online 21 MAR 2014

Autofluidization of pyroclastic flows propagating on rough substrates as shown by laboratory experiments

Corentin Chedeville[1,2,3] and Olivier Roche[1,2,3]

[1]Laboratoire Magmas et Volcans, Clermont Université, Université Blaise Pascal, Clermont-Ferrand, France, [2]CNRS, UMR 6524, LMV, Clermont-Ferrand, France, [3]IRD, R 163, LMV, Clermont-Ferrand, France

Abstract This study investigates the influence of the substrate surface roughness on the emplacement mechanisms of pyroclastic flows. We carried out laboratory experiments on gravitational flows generated from the release of initially fluidized or nonfluidized columns of fine particles (diameter $d = 0.08$ mm) in a horizontal channel. The roughness of the channel base was uniform in each experiment, created by gluing particles of diameter $d_0 = 0.08$ to 6 mm to the base. Other things being equal, the flow runout distance increased with the channel base roughness (d_0) to a maximum of about twice that of flows on a smooth substrate when $d_0 = 1.5$–3 mm, before decreasing moderately at higher roughness values of $d_0 = 6$ mm. Long runout originated mainly during the late stages of emplacement as flow deceleration was strongly reduced at high substrate roughness. This was caused by (partial) autofluidization due to an upward air flux escaping from the substrate interstices in which flow particles settled. Autofluidization was evidenced by high pore fluid pressure measurements at the base of initially nonfluidized flows and also by reduced flow runout when the interstices were initially partially filled so that less air was available. Furthermore, the runout distance of flows of large particles ($d = 0.35$ mm), which could not be fluidized by the ascending air flux, was independent of the substrate roughness. This study suggests that autofluidization caused by air escape from the interstices of a rough substrate is one important mechanism to explain the common long runout distance of pyroclastic flows even on subhorizontal topographies.

1. Introduction

Pyroclastic flows represent the dense gravity-driven mixture of gas and solid particles at the base of many pyroclastic density currents [*Cas and Wright*, 1987; *Druitt*, 1998; *Freundt et al*., 2000]. They are commonly generated from the gravitational collapse of an unstable eruptive column [e.g., *Sparks and Wilson*, 1976] or a lava dome [e.g., *Cole et al*., 1998], but secondary pyroclastic flows may also result from detachment and rapid sedimentation of the dilute surge component of a pyroclastic density current [*Druitt et al*., 2002]. The ability of many pyroclastic flows to propagate on subhorizontal slopes over distances of several kilometers and the density segregation of clasts in their deposits suggests that they are gas-fluidized mixtures [*Sparks*, 1976; *Wilson*, 1980]. In this context, the emplacement mechanisms and the runout of pyroclastic flows are likely to be controlled principally by the longevity of the gas sources and the process of pore fluid pressure diffusion [*Druitt et al*., 2007; *Roche et al*., 2010; *Roche*, 2012]. The interstitial gas can be of primary (i.e., volcanic) or external origin. In the latter case, *Wilson* [1980] proposed that air can be ingested at the flow front and that gases can be released when a pyroclastic flow travels over water or burns vegetation.

A major issue related to the hazards posed by pyroclastic flows is that the flow runout distance is difficult to predict, because it is controlled by a large number of flow properties (volume, velocity, gas content, and clast size distribution) as well as by topography. The latter can be particularly critical because, in addition to the slope variation, pyroclastic flows propagate on substrates that can have a highly variable surface roughness (Figure 1), and this may be an important factor in controlling the emplacement mechanisms (see the recent study of *Roche et al*. [2013] using an erodible granular substrate). The present study addresses this issue through a series of laboratory experiments on granular flows propagating on a nonerodible substrate of variable surface roughness. Previous experimental studies involved flows of particles of relatively large grain size ($d \sim 0.1$–1 mm) and substrate roughness of the same order [*Pouliquen*, 1999; *Goujon et al*., 2003; *Lajeunesse et al*., 2004; *Lube et al*., 2011]. In contrast, we consider here flows of finer particles and a large range of substrate roughness. We investigate how the latter controls the emplacement mechanisms of the flows

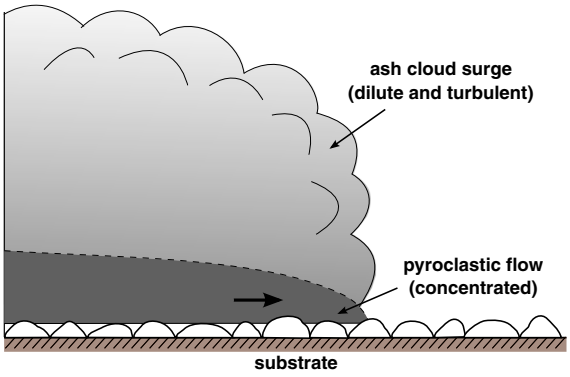

Figure 1. Sketch of a pyroclastic density current. A basal pyroclastic flow with high particle concentration propagates over an irregular rough substrate and is overridden by a dilute ash cloud surge. The dashed line represents the transition (sharp or diffuse) between the flow and the surge components.

and their runout distance in particular. This is achieved through dam break experiments on initially fluidized or nonfluidized granular flows propagating over a horizontal rough substrate, thus extending earlier studies involving a smooth substrate [e.g., *Roche et al.*, 2006, 2008; *Girolami et al.*, 2008, 2010].

2. Experimental Methods and Device

2.1. Principles of Pore Fluid Pressure Generation and Diffusion

High pore fluid pressure, causing fluidization of pyroclastic flows through drastic reduction of interparticle frictional forces, can be generated by relative vertical motion between the interstitial gas and the particles. This occurs when an upward gas flux is provided and/or when the particles settle in dense mixtures. In laboratory experiments, pore pressure is generated by injecting air at the base of a static and compacted granular column (Figure 2). Full fluidization is achieved at the minimum fluidization velocity, U_{mf}, when the drag force caused by the interstitial gas flow counterbalances the apparent weight of the particles, so that the pore fluid pressure is equal to the lithostatic pressure defined as

$$P = [\rho_s \varepsilon_s + \rho_f (1 - \varepsilon_s)] g H, \tag{1}$$

where ρ_s and ρ_f are the particle and gas density, respectively, ε_s is the particle concentration, g is the gravity acceleration, and H is the bed height [*Rhodes*, 1998]. Note that as $\rho_f << \rho_s$, then equation (1) can be simplified as

$$P \approx \rho_s \varepsilon_s g H. \tag{2}$$

If the gas flux is no longer supplied and there is no relative gas-particle motion (Figure 2c), the pore pressure then decreases with time (t) according to a diffusion law described by

$$\frac{\partial P}{\partial t} = D \frac{\partial^2 P}{\partial z^2}, \tag{3}$$

where z is the bed height and D is the hydraulic diffusion coefficient [*Iverson*, 1997]. Hence, the granular material remains (partially) fluidized during the process of pore pressure diffusion, whose time scale (Δt) increases with H^2/D and with decreasing particle grain size (i.e., low D values). At the laboratory scale, for H of the order of 1–10 cm, Δt is typically a few seconds for beds of fine group A particles (grain size < ~0.1 mm) of *Geldart*'s classification [*Geldart*, 1986] but is almost negligible for beds of larger particles (groups B–D). Note that initial gas velocity greater than U_{mf} causes homogeneous expansion of beds of group A particles, which notably increases Δt compared to nonexpanded beds owing to particle settling [*Montserrat et al.*, 2012; *Roche*, 2012].

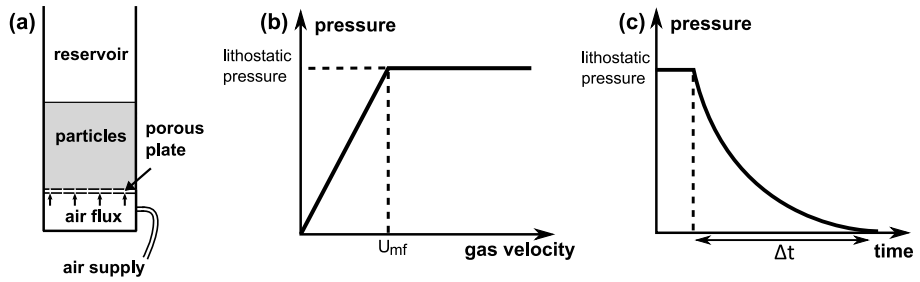

Figure 2. (a) Generation of pore fluid pressure in a bed of particles fluidized by injecting air from below. (b) Pore pressure as a function of the gas velocity, equal to the lithostatic pressure at U_{mf}. (c) Diffusion of pore pressure if gas supply is no longer provided, where Δt is the duration of pore pressure diffusion. This applies to flows in our experiments since no air flux is provided from the channel base.

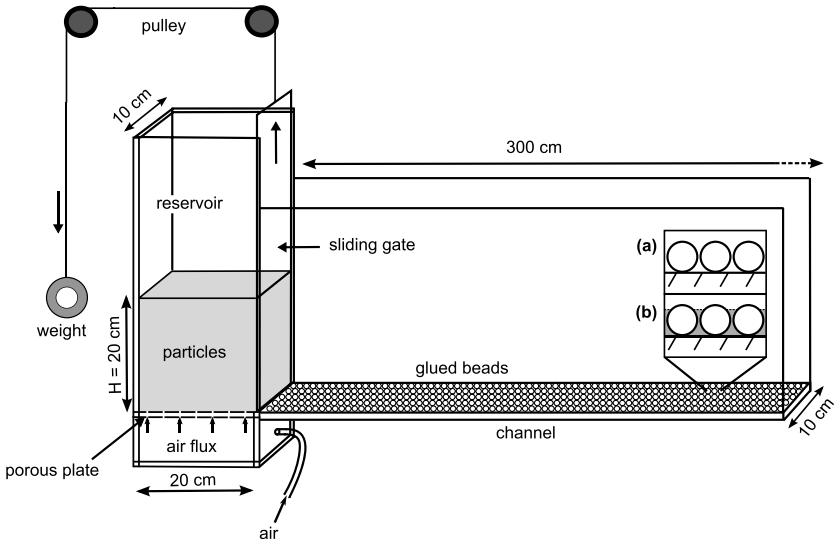

Figure 3. Experimental device consisting of a (fluidization) particle reservoir and a horizontal channel whose base is roughened by glued beads (not to scale). The inset shows (a) glued beads alone and (b) with their interstices partly filled by either PEG or fine beads (gray).

2.2. Experimental Device

We carried out dam break experiments in an apparatus consisting of a particle reservoir and a horizontal channel whose base was covered with glued glass beads (Figure 3). Removal of the reservoir gate by means of a counterweight permitted the rapid release of 6 kg of particles, corresponding to an initial column height of $H = 20$ cm, which led to a gravitational granular flow in the channel. The flows were filmed with a high-speed video camera at rates of 60 frames/s for investigating the general flow emplacement and up to 3800 frames/s for detailed views.

The flow particles were nearly spherical glass beads with a density of 2500 kg m^{-3}. Most experiments were carried out with fine group A particles of mean grain size $d = 0.08$ mm (range 0.06–0.09 mm) to respect dynamic similarity with pyroclastic flows [*Roche*, 2012]. Before each run, the particles were dried for 10 min in a fluidization rig in order to avoid possible minor cohesion effects due to ambient moisture. In some experiments, particles were fluidized in the reservoir by injected air through a basal porous plate. The mean air flow velocity was 14 mm s^{-1}, above U_{mf} of 8.3 mm s^{-1} [*Roche et al.*, 2006], which led to homogeneous, slightly (~5%) expanded beds. As no gas flux was provided from the channel base, the subsequent flow then defluidized through pore pressure diffusion during propagation (cf. Figure 2c). Complementary experiments were carried out with group B particles of mean grain size $d = 0.35$ mm (range 0.25–0.43 mm). As initial fluidization of such large particles has a negligible influence on flow emplacement at laboratory scale because of nearly instantaneous pore pressure diffusion [*Roche et al.*, 2006], only initially nonfluidized flows were considered for these particles.

Variation of the surface roughness of the channel base was obtained by changing the mean grain size of the glued beads ($d_0 = 0.08$, 0.2, 0.35, 0.5, 0.7, 1.5, 3.0, and 6.0 mm). These particles were randomly distributed, though hexagonal arrangements were often observed for the largest ones. The term *roughness* used hereafter designates the size of the glued beads. Additional experiments with flows propagating on a smooth substrate (without glued beads) were also carried out for comparison. For each substrate roughness, experiments were repeated at least 7 times for initially fluidized flows and at least 3 times for nonfluidized flows. In complementary experiments involving a substrate roughness of 3 mm, the interstices between the glued beads were filled to about 80% of their height (Figure 3). This was achieved by adding either (i) fine beads of 0.08 mm, leveled with a brush before each experiment, or (ii) molten polyethylene glycol (PEG) that solidified at ambient temperature.

Sensors were used to measure pore fluid pressure at the base of the flows (see *Roche et al.* [2010] for technical details). They were covered by a 36 μm grid that prevented contact with the flow particles but permitted pore pressure transmission to the sensory membrane. In such experiments, 12 kg of particles were released from

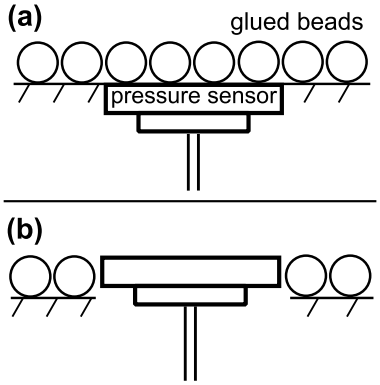

Figure 4. Pressure sensors positioned (a) at the base of the channel, with beads glued on the grid covering the sensor (method 1), and (b) at the same level as the top of the beads glued on the channel base (method 2).

the reservoir ($H \sim 40$ cm) in order to obtain thick flows and hence large pressure signals. Pressure measurements were made for both initially fluidized and nonfluidized flows on both smooth and rough substrates ($d_0 = 3.0$ mm). In the latter case, the upper part of the sensor was positioned either at the channel base (below the glued beads) or the top of the glued beads (Figure 4).

2.3. Scaling Issues

A detailed dimensional analysis of the experiments presented in *Roche* [2012] accounts for the degree of dynamic similarity between pyroclastic flows and their laboratory analogs. The choice of particle type (i.e., the groups in Geldart's classification) is crucial regarding dynamic similarity between both types of flows. Here fine particles of group A are representative of the ash matrix of many pyroclastic flows [*Druitt et al.*, 2007] and are used to investigate their emplacement. With such fine particles, dimensionless numbers for both types of flows generally have close values, or at least indicate the same physical regimes. Experimental flows, however, are likely to defluidize through pore pressure diffusion at a relatively faster rate than most pyroclastic flows, because they are thinner (see equation (3)). In this paper we add the substrate roughness (d_0) as another physical parameter to the analysis of *Roche* [2012], which leads us to define an additional dimensionless number. We define the *roughness number*

$$Ro = \frac{h}{d_0}, \tag{4}$$

where h is the flow thickness. Comparing the Ro values in both nature and experiments, our analog flows of typical thickness $h \sim 3$ cm simulate propagation of 1 m or 10 m thick pyroclastic flows on a substrate having a roughness of ~0.003–0.2 m or ~0.03–2 m, respectively, which may be representative of most natural configurations.

3. Results

3.1. Flow Runout Distance

The runout distance of both initially fluidized or nonfluidized flows of particles of size $d = 0.08$ mm increased with the substrate roughness until the latter was 1.5–3 mm, at which point the runout was about twice that on a smooth substrate (Figure 5). The runout then decreased by ~15–25% at the highest level of roughness

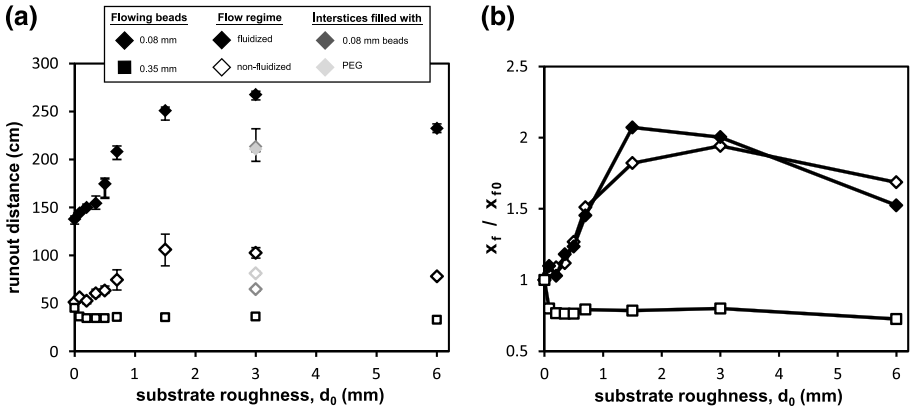

Figure 5. Runout distance of granular flows as a function of the substrate surface roughness (d_0). Results of complementary experiments at a roughness of 3 mm with interstices partially filled are also shown for both initially fluidized and nonfluidized flows of particles of size $d = 0.08$ mm. (a) Raw data. (b) Runout distance (x_f) normalized to the runout of flows on a smooth substrate (x_{f0}). Error bars can be smaller than symbols.

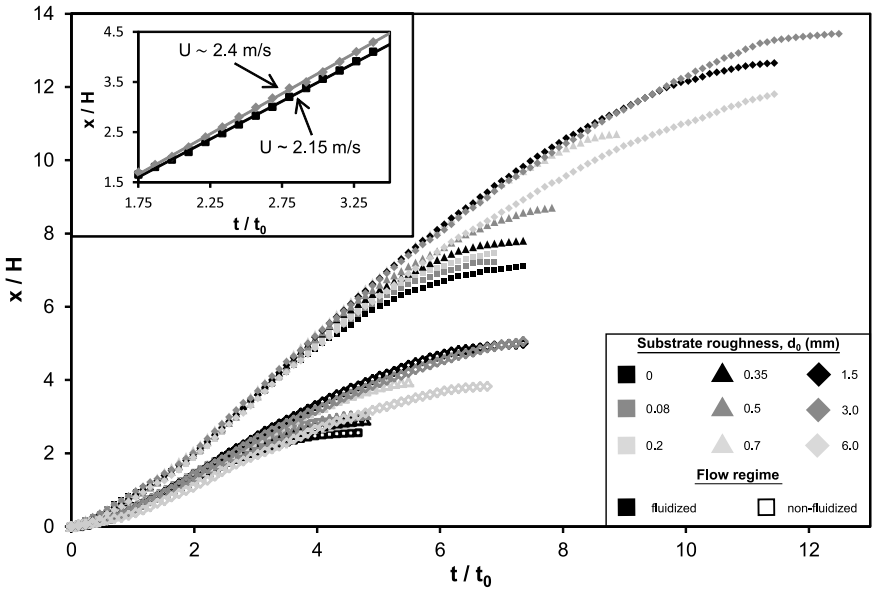

Figure 6. Front kinematic data of initially fluidized (filled symbols) and nonfluidized (open symbols) flows of particles of 0.08 mm on substrates of different roughness. The front position normalized to the initial column height (H) is represented as a function of time normalized by $t_0 = (H/g)^{1/2}$. The inset represents a detailed view of the data for initially fluidized flows on smooth or 3 mm rough substrates during the intermediate constant velocity phase.

investigated ($d_0 = 6$ mm). In experiments with a roughness of 3 mm, partial filling of the interstices led to shorter runout distances compared to a substrate with uniform-sized glued beads alone. The runout decrease was ~20% or ~20–35% when interstices were filled with PEG or fine glass beads, respectively. In the latter case, results were less reproducible probably because of slight changes in amount of filling between the experiments due to the protocol used (leveling with a brush).

In contrast to fine particle flows, flows of beads of size $d = 0.35$ mm had runouts almost independent of the roughness but ~20% shorter than on a smooth substrate. However, flow runout for the highest level of roughness investigated ($d_0 = 6$ mm) was only slightly shorter than for smoother substrates.

3.2. Flow Front Kinematics

The kinematics of flows of fine particles ($d = 0.08$ mm) were investigated as a function of the substrate roughness. In Figure 6, the normalized flow front position in the channel, x/H, is shown as a function of the normalized time, $t/(H/g)^{1/2}$, where the initial column height H is the relevant length scale parameter and g is the gravitational acceleration [*Roche et al.*, 2008]. Earlier works showed that dam break granular flows on smooth substrates propagated in three distinct phases according to these dimensionless parameters [e.g., *Lajeunesse et al.*, 2004; *Roche et al.*, 2008]. The flows first accelerated, then propagated at nearly constant front velocity for most of their emplacement, and finally decelerated. For flows of fine group A particles that were initially fluidized, the constant front velocity $U_f \sim (2gH)^{1/2}$ was equal to that of inertial flows of single phase fluids, reflecting sustained high pore fluid pressure due to slow diffusion [*Roche et al.*, 2008]. Deceleration began when pore pressure had decreased sufficiently for particle interactions to significantly dissipate the flow energy [*Roche et al.*, 2010].

In our experiments, the front kinematics of both initially fluidized and nonfluidized flows of fines were independent of the substrate roughness until transition to the decelerating phase, which occurred at $t/(H/g)^{1/2} \sim 3.75$–4 and ~2–2.5, respectively (Figure 6). However, the constant velocity of initially fluidized flows, during the second phase of emplacement, increased slightly with the substrate roughness. For instance, it varied from 2.15 m s^{-1} for a smooth substrate to 2.40 m s^{-1} for a 3 mm rough substrate (Figure 6, inset). The main differences in flow kinematics arose at a late stage, with lower flow deceleration as the substrate roughness increased, hence leading to longer flow runout and duration. The latter two reached a maximum at a roughness between 1.5 and 3 mm and were about twice that for a smooth substrate. For the highest roughness investigated ($d_0 = 6$ mm), the front velocity, runout, and duration of both initially fluidized and nonfluidized flows were slightly lower than for 1.5 mm and 3 mm rough substrates but remained greater than for smoother substrates.

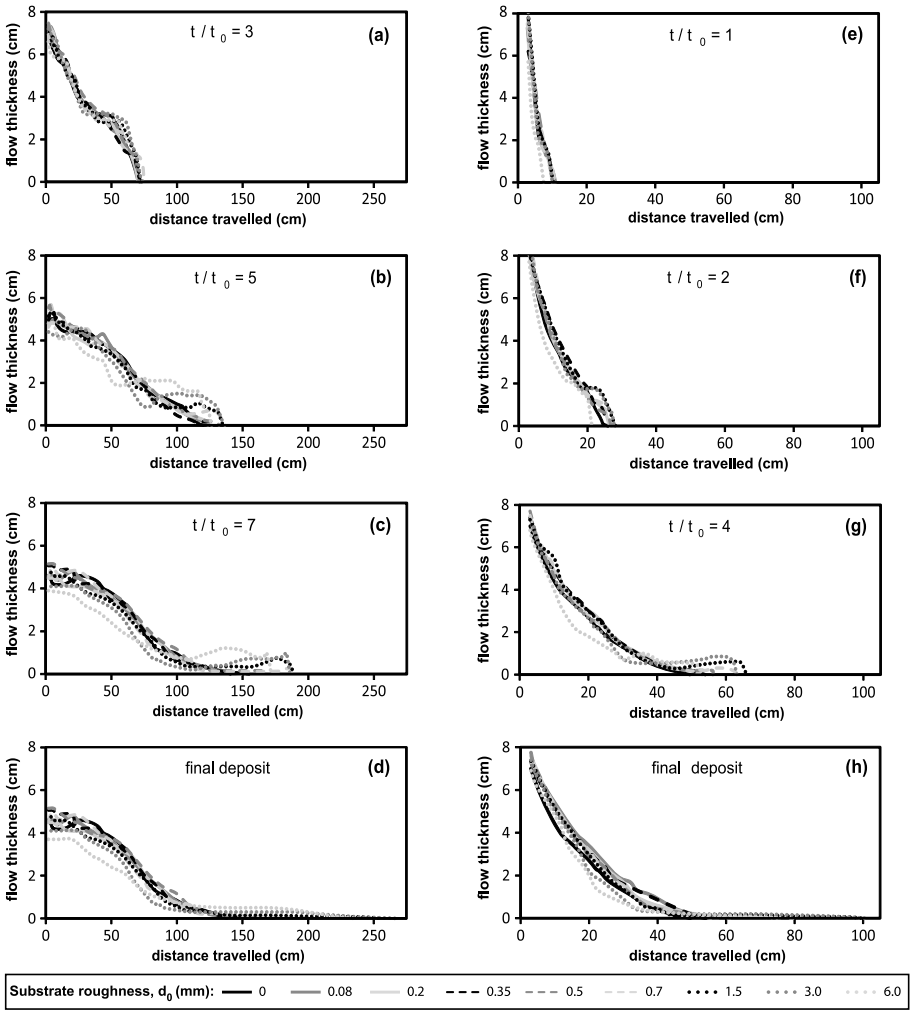

Figure 7. Morphology of initially (a–d) fluidized and (e–h) nonfluidized flows of particles of size $d = 0.08$ mm, at different times of propagation. According to Figure 6, t/t_0 is the normalized time. The flow head becomes humped at the beginning of the deceleration phase (Figures 7b and 7f), and both its length and height increase with the substrate roughness. At later stages, the flow head stretches horizontally until the flow comes to halt (Figures 7d and 7h).

3.3. Flow Morphology

Both initially fluidized and nonfluidized flows of fine particles ($d = 0.08$ mm) consisted of a sliding head (i.e., with nonzero basal velocity) and a body, at the base of which deposition occurred incrementally [*Roche et al.*, 2010; *Girolami et al.*, 2010; *Roche*, 2012]. As in the case of the front kinematics, the flow morphology did not depend on the substrate roughness at early stages of propagation (Figure 7, see Movies S1–S4 in the supporting information). However, during the decelerating phase, both the height and length of the flow head increased with the roughness, while the shape of the flow body was little affected. During the final

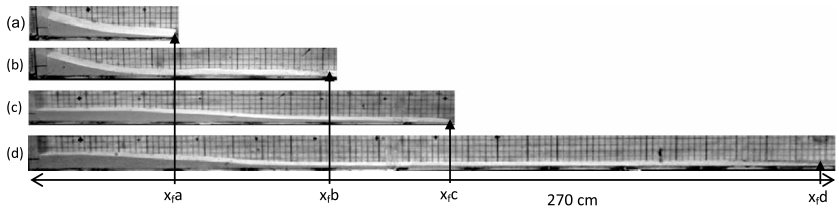

Figure 8. Deposits of initially nonfluidized flows (a) on smooth substrate and (b) on 3 mm rough substrate, and of initially fluidized flows on (c) smooth substrate and (d) 3 mm rough substrate. The flow runout distance in each case is x_f.

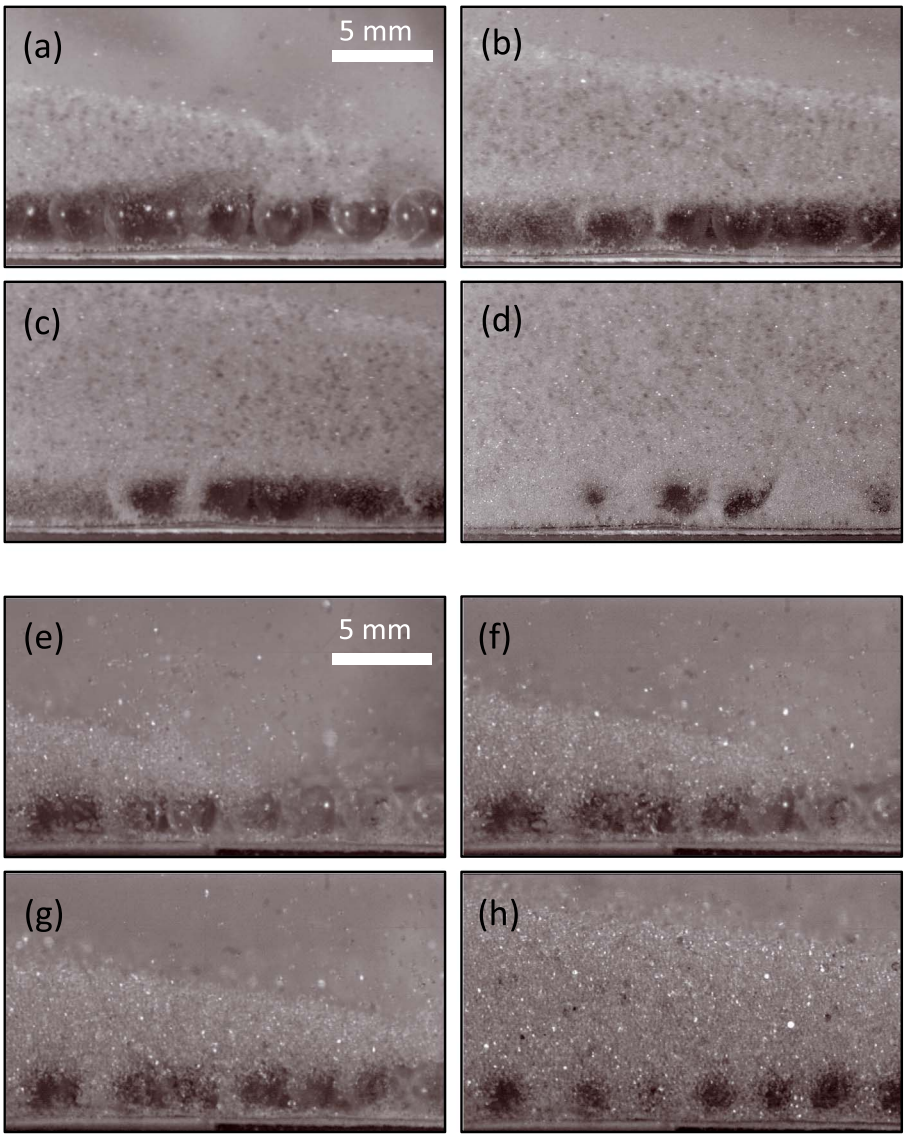

Figure 9. Snapshots of an initially fluidized flow of particles of size $d = 0.08$ mm propagating over a 3 mm rough substrate, at 100 cm from the reservoir. (a) Front arrival at time t_0, (b) $t = t_0 + 0.008$ s, (c) $t = t_0 + 0.016$ s, and (d) $t = t_0 + 0.09$ s. Larger black particles ($d = 0.2$ mm) were used as markers at a proportion of 1–2% of the total particle weight. Snapshots of a flow of particles of size $d = 0.35$ mm propagating on a 3 mm rough substrate at 25 cm from the gate. (e) Front arrival time at t_0, (f) $t = t_0 + 0.008$ s, (g) $t = t_0 + 0.016$ s, and (h) $t = t_0 + 0.065$ s.

stage, the main body rapidly stopped moving but the head still propagated and stretched horizontally. The amount of stretching increased with the substrate roughness, thus leading to thin (<1 cm) distal deposits (Figure 8, see Movies S3 and S4 in the supporting information) with an almost horizontal (<1°) upper surface and causing the long flow runout distances reported in Figures 5 and 6.

3.4. Flow-Substrate Interaction

The mechanisms of interaction between the granular flows and their substrate were investigated using high-speed videos (Figure 9). The head of both initially fluidized and nonfluidized flows of fine particles ($d = 0.08$ mm) slid over the substrate. Following this phase, dense clusters of flow particles dropped into the substrate interstices. Settling velocities were measured either at the base of the clusters or by tracing the markers (larger black particles) inside these clusters, with no significant difference between these two methods. We obtained settling velocities of ~80–200 mm s^{-1} for a 3 mm rough substrate, with the highest values approaching the free-fall velocity for a height of 3 mm. Note that observations were made at the

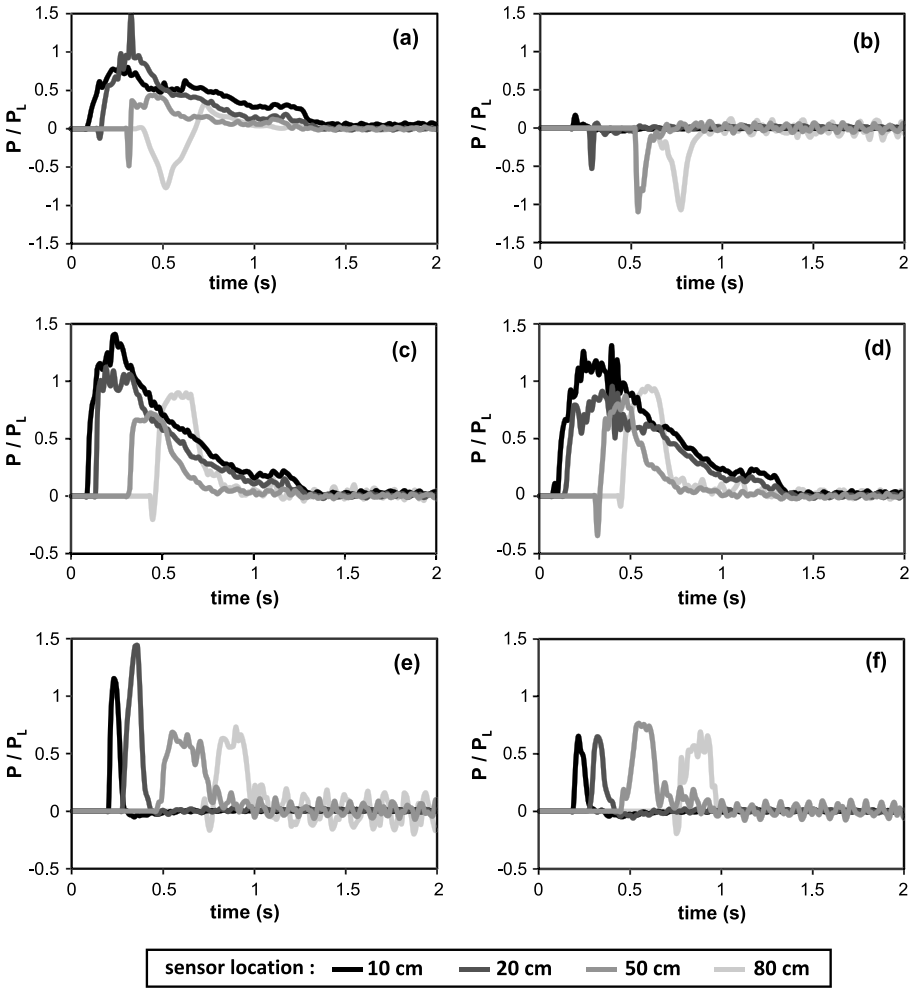

Figure 10. Basal pore pressure P normalized to the lithostatic pressure $P_L = \rho_s \varepsilon_s g h$, with $\rho_s \varepsilon_s$ the bulk density of the flow (~1450 kg/m^3), g the gravitational acceleration, and h the flow thickness over the sensor, as a function of time. Time zero corresponds to flow initiation at gate opening, and pore pressure was measured at various distances from the gate according to methods 1 and 2 shown in Figure 4. Results are shown for flows propagating on smooth substrate and which are (a) initially fluidized or (b) nonfluidized flows, flows propagating on 3 mm rough substrate and which are initially fluidized, with (c) method 1 and (d) method 2, or nonfluidized, with (e) method 1 and (f) method 2. Note that the normalization of negative pore pressure values to the lithostatic pressure has no physical meaning here; these values are only preserved to show that underpressure occurs at the flow front.

channel side and that particle settling velocities could have been different for an unconfined substrate. The duration of this phase of infilling of the interstices increased with the roughness. For example, it varied from ~0.06 s to ~0.11 s for a roughness of 0.7 mm to 3 mm, respectively, which corresponded to a travel distance of ~12.5 to 22 cm for initially fluidized flows and of ~7 to 15 cm for nonfluidized ones. For flows of particles of size $d = 0.35$ mm, intense collisions with the substrate were observed at the flow base. For a substrate roughness ≥ 1.5 mm, particles dropped as dilute clusters into the interstices immediately after the passage of the flow front, at velocities of ~80–140 mm s^{-1} (Figures 9e–9h).

3.5. Basal Pore Pressure

Results of pore pressure measurements at the base of flows of particle size $d = 0.08$ mm are presented in Figure 10. The data for flows on a smooth substrate are similar to those reported in earlier studies [*Roche et al.*, 2010; *Roche*, 2012] and are shown here for comparison with cases involving rough substrates. The sliding head of the flows generated under pressure proportional to the front velocity, whereas pore pressure transmitted by the flow body depended on the initial conditions [*Roche*, 2012; *Roche et al.*, 2013]. In the case of initially fluidized flows, pore pressure was high during the early stages (i.e., close to the reservoir), because

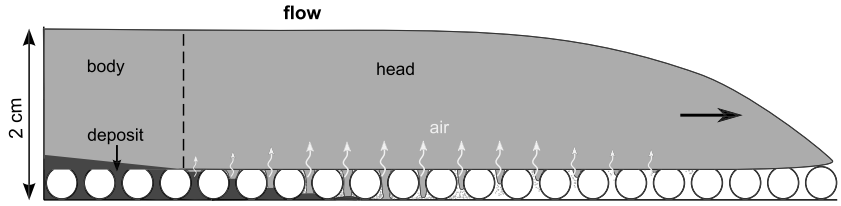

Figure 11. Schematic representation of the autofluidization process for a flow of fine particles propagating on a rough substrate. The air escapes from the substrate interstices, into which flow particles settle, and percolates upward through the flow.

it was advected rapidly from the reservoir and had not yet diffused much. This explains why pore pressure could be higher than the lithostatic pressure for a given flow depth [*Roche et al*., 2010]. Pressure then decreased through diffusion until the flow was totally defluidized. In contrast, initially nonfluidized flows did not generate overpressure. An exception occurred at 10 cm from the reservoir where up to ~16% of the particle weight was supported for a very short duration (Figure 10b), possibly due to some compaction causing differential air-particle motion as the material was released from the reservoir [*Roche et al*., 2010].

On a 3 mm rough substrate, initially fluidized flows generated pressure signals similar to those on a smooth base during the first stage (at 10–20 cm from the reservoir). However, during the intermediate stage, overpressure supported ~70–90% of the particles' weight at distances of up to 80 cm (Figures 10c and 10d). In comparison, less than 50% of the particle weight was supported at that stage on a smooth substrate. Another notable difference was that underpressure was small and of short duration for the rough substrate, particularly when the sensors were located below the glued beads (see method 1 in Figure 4). For initially nonfluidized flows (Figures 10e and 10f), the pressure signals differed fundamentally from those observed for a smooth substrate. Overpressure was high at all stages of the flow, with at least ~70% of the particles' weight supported. For instance, nearly full bed support was detected even at a distance of 80 cm from the reservoir, whereas the flow runout was 130 cm. Note that the duration of overpressure increased significantly between the early (at 10 and 20 cm) and intermediate to late stages (at 50 and 80 cm), showing that an increasing part of the flow had high pore pressure. Furthermore, at late stages, this duration was almost equal to that of initially fluidized flows.

4. Discussion

4.1. Flow Mechanisms in Experiments

Our results showed that the runout of both initially fluidized and nonfluidized flows of group A fine particles ($d = 0.08$ mm), propagating on a rough substrate, was increased by up to a factor of ~2 in comparison with a smooth base. Kinematic and morphological data revealed that the increase of runout was acquired mostly during the decelerating phase, as more material was transferred to the flow head, which then spread considerably to form a thin and elongated deposit (Figures 7 and 8). High pore pressure at the base of initially nonfluidized flows of fines on a rough substrate proved that autofluidization occurred during emplacement. We propose that this was caused by flow particles dropping into the substrate interstices, causing an upward flux of escaping air (Figure 11). Even if the flow particles did not fall entirely into the substrate interstices at the lowest roughness investigated (as low as $d_0 = 0.08$ mm), the small amount of air evacuated could have caused the slight runout increase compared to a smooth substrate. This autofluidization mechanism is different from that proposed by *Bareschino et al*. [2008] for flows generated in a rotating drum for which "plunging breakers" collapsed at the front and forced the ambient air to percolate through the flow. In our experiments, the velocity of the upward air flux can be estimated from volume conservation consideration. We consider the volume flux

$$Q = SU, \tag{5}$$

where U is the velocity and S the cross-sectional area. With Q_p and Q_{ia} the volume flux of the settling particles and of the interstitial air, respectively, and stating $Q_p = Q_{ia}$ then

$$\varepsilon_p U_p = \left(1 - \varepsilon_p\right) U_{ia}, \tag{6}$$

with ε_p the particle volume fraction. The interstitial air velocity, however, has to be converted into a superficial air velocity (U_{sa}) in order to be compared with U_{mf}, so that

$$U_{sa} = \left(1 - \varepsilon_p\right) U_{ia}. \tag{7}$$

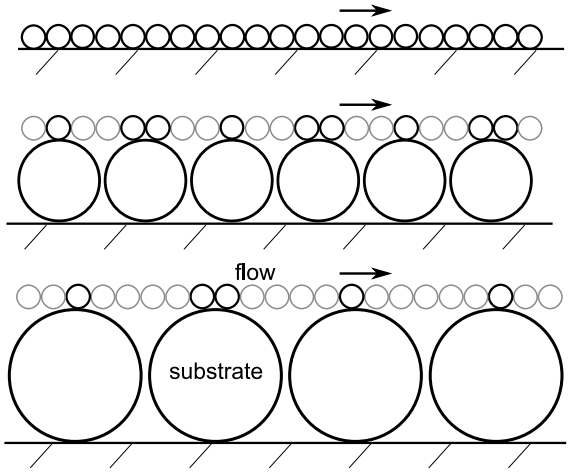

Figure 12. Schematic representation of the contacts (black circles) between the particles at the base of the flow head and a (a) smooth, (b) moderately rough, and (c) very rough substrate.

Combining equations (6) and (7) leads to

$$\varepsilon_p = U_{sa}/U_p. \quad (8)$$

In this context, settling clusters (at velocities of ~80–200 mm s^{-1}) with particle volume fractions as low as ~0.1 would cause air escape velocities higher than the minimum fluidization velocity (U_{mf}) of the fine flow particles (~ 8 mm s^{-1}). Moreover, even upward air velocity less than U_{mf} can produce a drag force that reduces the internal friction and thus increases the flow runout, albeit less efficiently than U_{mf}. Note that as U_{mf} is length-scale independent, air escape velocity in nature similar to that estimated above is expected to cause fluidization of pyroclastic flows containing mainly ash (group A) particles with a mean grain size close to that in our experiments.

According to this autofluidization mechanism, the source of air in our experiments was available until the interstices were completely filled by the flow particles. In that circumstance only the frontal part of the flow could be fluidized. As the duration of the upward air flux increased with the volume of the substrate interstices, the length of this frontal part increased with the roughness. This is consistent with the fact that the amount of stretching of the flow head increased with the roughness, whereas the morphology of the flow body was almost unchanged. For a given substrate roughness, rapid filling of the interstices close to the reservoir, due to some vertical velocity component of the collapsing granular column, may explain the relatively short duration of overpressure (Figure 10). On the other hand, slower filling at greater travel distances, where the material propagated horizontally, is consistent with the observed longer overpressure phase. The autofluidization hypothesis is also supported by the experiments with the substrate interstices partially filled with PEG or small beads before the flow was generated, because volume reduction of the air available caused a significant decrease (~20–35%) of runout for a given substrate roughness.

In the case of initially fluidized flows, air escape from the substrate interstices contributed to delayed diffusion of pore pressure derived from the reservoir. The pressure measurements suggest that the effect of this additional source of gas was negligible at early flow stages, when initial pore pressure had not decreased much, but became very marked at longer travel distances because pore pressure was significantly higher than for a smooth substrate (see data at 50 cm and 80 cm in Figure 10). For a given roughness, autofluidization increased the flow runout, compared to a smooth substrate, in the same proportion as for initially nonfluidized flows.

The flow runout at the highest substrate roughness of 6 mm was shorter than at an intermediate roughness of 1.5–3 mm (Figure 5) despite the fact that more fluidizing air was available from the interstices. Close examination of the kinematic data revealed that both initially fluidized and nonfluidized flows on a 6 mm rough substrate had a lower velocity than flows on smoother substrates, from the start of propagation (Figure 6). This can be explained by the fact that, as the size of the interstices increased, the flow particles were less able to move over the beads forming the substrate: first, the large glued beads could act as obstacles to flow propagation as many flow particles collided with them, dissipating flow energy, and second, as more flow particles fell into the interstices, the flow head lost its mass and thus spread less. These two mechanisms could have caused the decrease of flow runout compared to intermediate substrate roughness.

Another mechanism may have contributed to the control of the flow propagation and runout. Experiments of *Géminard and Losert* [2002], involving a horizontal plate sliding on a flat granular material, showed that the dynamic friction coefficient decreased by up to ~40% when the roughness of the granular layer (i.e., the size of the particles) increased by a factor of about 4. *Pohlman et al.* [2006] also observed a decrease in the friction coefficient with increasing substrate roughness for their rotating drum experiments. Based on these studies and considering the sliding head of fine particle flows in our experiments as a continuous medium (see Figures 9a and 9b), the friction between the flow base and the substrate may have been reduced as the roughness

increased. This could be related to the fact that the contact area per unit length between the flow base and the substrate decreased as the roughness (and thus the size of the interstices) increased (Figure 12), hence leading to lower energy dissipation. This reduction of friction was probably negligible compared to the autofluidization mechanism discussed above in accounting for the strong variation in flow runout. It may, however, explain the increase of flow velocity with increased substrate roughness at early flow stages (Figure 6).

The flows of particles of size $d = 0.35$ mm are difficult to fluidize because U_{mf} for these large particles is high (99.5 mm s^{-1}) [after *Roche et al*., 2006]. Furthermore, rapid filling of the interstices (Figures 9e–9h) and thus short duration of the associated air flux, coupled with the high permeability of these clusters of large particles (group B) that cause rapid pore pressure diffusion, would have prevented autofluidization of the flow. Hence, the size of the interstices, which controlled the duration of air escape, did not have any influence on the runout distance. Note that *Bareschino et al*. [2008] reported the absence of autofluidization in their experiments involving large beads of size $d = 0.55$ mm. The almost constant runout of flows of these coarse particles in our experiments suggests that the amount of energy dissipation, through interactions between the flow particles and the substrate, was about the same for the different roughnesses. This is consistent with the fact that the flow head did not slide on the substrate as a continuous medium; instead, the flow particles collided with the substrate beads and began to settle in the interstices almost immediately after the passage of the flow front. Longer runout distances of flows on a smooth substrate may suggest lower energy dissipation. Rolling of flow particles (particularly at the flow front) may have contributed to these longer runouts compared to rough substrates.

4.2. Implication for Pyroclastic Flows

Our results suggest that ash-rich pyroclastic flows, whose matrix consists of fine group A particles, can be autofluidized when they propagate on a rough, horizontal substrate. In nature, it is likely that flow particles will fall into the substrate interstices sufficiently rapidly to cause air escape at velocities greater than the U_{mf} of the pyroclastic material, which can be as low as 1 mm s^{-1} [*Druitt et al*., 2007]. According to our experiments, which show the highest runout values for flows of ~3 cm thick on substrates of roughness 1.5–3 mm, and assuming the same values of *Ro* in experiments and nature, the autofluidization of 1 m to 10 m thick pyroclastic flows is expected to cause maximum runout (other things being equal) at mean substrate roughness of 0.05–0.1 m to 0.5–1 m, respectively.

Although more air would be available to fluidize pyroclastic flows at greater roughness, large surface irregularities would actually act as obstacles, and flows would lose much of their mass through sedimentation in the interstices. In contrast to these fines-rich flows, the behavior of scoria or coarse-grained pumice flows would be unaffected by air escape from the substrate and their runout is expected to be independent of the substrate roughness. Irrespective of the flow type and nature of the substrate, propagation on steep slopes may occur in a manner different from that described above and we acknowledge that this issue deserves further investigation.

The present study also has implications for models of pyroclastic flows because any source of fluidizing air at the flow base will be essential in controlling the flow dynamics [e.g., *Iverson et al*., 2004; *Denlinger and Iverson*, 2004]. In particular, a basal air flux will increase the pressure diffusion time scale so that flow propagation will be favored.

5. Conclusions

Our experiments were carried out with fine ($d = 0.08$ mm) group A particles that are representative of the ash matrix of many pyroclastic flows. They showed that flows propagating on horizontal rough substrates were autofluidized by air escaping from the interstices during the particle settling, which caused longer runout distances than in the case of smooth substrates. Such a counterintuitive relationship between flow runout and substrate roughness was also reported by *Andrews and Manga* [2012] for dilute turbulent currents whose physics are fundamentally different from those of the dense gas-particle mixtures we considered. In our experiments, autofluidization was evidenced in initially nonfluidized flows with high pore fluid pressure supporting at least ~70% of the particle weight. Other things being equal, the flow runout increased with the substrate roughness because the volume of air available was proportional to the size of the interstices so that the flows were fluidized for a longer duration. The runout increase was most marked at late stages of emplacement. It occurred as autofluidization permitted more material to be transferred to the flow head, which spread to form a thin (<1 mm), elongated deposit with a very small surface slope (<1°). The longest runout, about twice that for a smooth substrate, was at a roughness of 1.5–3 mm. At the highest roughness

value of 6 mm, however, substrate irregularities acted as obstacles and the mass of the flow decreased significantly through sedimentation into the substrate interstices, which caused a shorter runout even though more air was potentially available in the interstices. In contrast, the flow runouts of large ($d = 0.35$ mm) group B particles, which could not be autofluidized, were independent of substrate roughness.

This investigation suggests that air present in topographic lows of a natural substrate should be considered as another external source of gas that can fluidize pyroclastic flows, along with air ingested at the front of the flow or gas resulting from water vaporization or burnt vegetation [cf. *Wilson*, 1980; *Bareschino et al*., 2008]. Important implications of our study are that (1) the autofluidization mechanism can contribute to causing long runout distances even on horizontal slopes and (2) ash-rich pyroclastic flows generated successively under similar initial eruptive conditions (i.e., volume, mass flux, drop height, grain size distribution, fluidization state, particle concentration…) during a volcanic crisis may have very different runout distances around an edifice depending on the roughness of the substrate on which they propagate. Scaling of our results to nature suggests that autofluidization can lead to the longest runout distances (other things being equal) when the mean substrate roughness is a few centimeters to a few tens of centimeters for 1 m to 10 m thick pyroclastic flows, respectively. Such roughness values are typical of the surface of many natural substrates, including those consisting of pyroclastic flow or fall deposits, debris avalanche deposits (apart from large hummocks), solidified lava flows, or even fluvial sediments. In this context, numerical simulations of pyroclastic flows should take the nature of the topography and possible fluidization effects caused by air escape from the substrate into careful consideration. The autofluidization mechanism evidenced by our study might also occur in other types of fines-rich geophysical flows characterized by a long runout distance, such as the Socompa debris avalanche [e.g., *van Wyk de Vries et al*., 2001]. We acknowledge, however, that this issue requires further investigation.

Acknowledgments

This work was supported by the Institut de Recherche pour le Développement (IRD, France). We thank Michael Barton and an anonymous reviewer for constructive comments. This is Laboratory of Excellence *ClerVolc* contribution 96.

References

Andrews, B. J., and M. Manga (2012), Counterintuitive effects of substrate roughness on PDCs, Abstract V11B-2753 presented at 2012 Fall Meeting, AGU, San Francisco, Calif., 3–7 Dec.

Bareschino, P., L. Lirer, A. Marzocchella, P. Petrosino, and P. Salatino (2008), Self-fluidization of subaerial rapid granular flows, *Powder Technol.*, *182*(3), 323–333, doi:10.1016/j.powtec.2007.12.010.

Cas, R. A. F., and J. V. Wright (1987), *Volcanic Successions, Modern and Ancient*, Allen and Unwin, London, U. K.

Cole, P. D., E. S. Calder, T. H. Druitt, R. Hoblitt, R. Robertson, R. S. J. Sparks, and S. R. Young (1998), Pyroclastic flows generated by gravitational instability of the 1996–1997 Lava Dome of Soufriere Hills Volcano, Montserrat, *Geophys. Res. Lett.*, *25*(18), 3425–3428.

Denlinger, R. P., and R. M. Iverson (2004), Granular avalanches across irregular three-dimensional terrain: 1. Theory and computation, *J. Geophys. Res.*, *109*, F01014, doi:10.1029/2003JF000085.

Druitt, T. H. (1998), Pyroclastic density currents, in *The Physics of Volcanic Eruptions*, Special Publications, vol. 145, edited by J. S. Gilbert and R. S. J. Sparks, pp. 145–182, Geological Society, London, U. K.

Druitt, T. H., E. S. Calder, P. D. Cole, R. P. Hoblitt, S. C. Loughlin, G. E. Norton, L. J. Ritchie, R. S. J. Sparks, and B. Voight (2002), Small-volume, highly mobile pyroclastic flows formed by rapid sedimentation from pyroclastic surges at Soufrière Hills Volcano, Montserrat: An important volcanic hazard, in *The Eruption of Soufrière Hills Volcano, Montserrat, From 1995 to 1999*, Geol. Soc. of London Mem., vol. 21, edited by T. H. Druitt and B. P. Kokelaar, pp. 263–279, Geological Society, London.

Druitt, T. H., G. Avard, G. Bruni, P. Lettieri, and F. Maez (2007), Gas retention in fine-grained pyroclastic flow materials at high temperatures, *Bull. Volcanol.*, *69*, 881–901.

Freundt, A., C. J. N. Wilson, and S. N. Carey (2000), Ignimbrites and block-and-ash flow deposits, in *Encyclopedia of Volcanoes*, edited by H. Sigurdsson, pp. 581–599, Academic Press. San Diego, Calif.

Geldart, D. (1986), *Gas Fluidization Technology*, Wiley, Chichester, U. K.

Géminard, J.-C., and W. Losert (2002), Frictional properties of bidisperse granular matter: Effect of mixing ratio, *Phys. Rev. E*, *65*, doi:10.1103/PhysRevE.65.041301.

Girolami, L., T. H. Druitt, O. Roche, and Z. Khrabrykh (2008), Propagation and hindered settling of laboratory ash flows, *J. Geophys. Res.*, *113*, B02202, doi:10.1029/2007JB005074.

Girolami, L., O. Roche, T. H. Druitt, and T. Corpetti (2010), Particle velocity fields in laboratory ash flows, *Bull. Volcanol.*, *72*(6), 747–759.

Goujon, C., N. Thomas, and B. Dalloz-Dubrujeaud (2003), Monodisperse dry granular flows on inclined planes: Role of roughness, *Eur. Phys. J. E Soft Matter*, *11*, 147–157.

Iverson, R. M. (1997), The physics of debris flows, *Rev. Geophys.*, *35*, 245–296.

Iverson, R. M., M. Logan, and R. P. Denlinger (2004), Granular avalanches across irregular three-dimensional terrain: 2. Experimental tests, *J. Geophys. Res.*, *109*, F01015, doi:10.1029/2003JF000084.

Lajeunesse, E., A. Mangeney-Castelnau, and J. P. Vilotte (2004), Spreading of a granular mass on a horizontal plane, *Phys. Fluids*, *16*, 2371–2381.

Lube, G., H. E. Huppert, R. S. J. Sparks, and A. Freundt (2011), Granular column collapses down rough, inclined channels, *J. Fluid Mech.*, *675*, 347–368.

Montserrat, S., A. Tamburrino, O. Roche, and Y. Niño (2012), Pore fluid pressure diffusion in defluidizing granular columns, *J. Geophys. Res.*, *117*, F02034, doi:10.1029/2011JF002164.

Pohlman, N. A., B. L. Severson, J. M. Ottino, and R. M. Lueptow (2006), Surface roughness effects in granular matter: Influence on angle of repose and the absence of segregation. *Phys. Rev. E*, *73*, 031304, doi:10.1103/PhysRevE.73.031304.

Pouliquen, O. (1999), Scaling laws in granular flows down rough inclined planes, *Phys. Fluids*, *11*, 542–548.

Rhodes, M. J. (1998), *Introduction to Particle Technology*, John Wiley, Chichester, U. K.
Roche, O. (2012), Depositional processes and gas pore pressure in pyroclastic flows: An experimental perspective, *Bull. Volcanol.*, *74*, 1807–1820.
Roche, O., M. A. Gilbertson, J. C. Phillips, and R. S. J. Sparks (2006), The influence of particle size on the flow of initially fluidized powders, *Powder Technol.*, *166*, 167–174, doi:10.1016/j.powtec.2006.05.010.
Roche, O., S. Montserrat, Y. Niño, and A. Tamburrino (2008), Experimental observations of water-like behavior of initially fluidized, dam break granular flows and their relevance for the propagation of ash-rich pyroclastic flows, *J. Geophys. Res.*, *113*, B12203, doi:10.1029/2008JB005664.
Roche, O., S. Montserrat, Y. Niño, and A. Tamburrino (2010), Pore fluid pressure and internal kinematics of gravitational laboratory air-particle flows: Insights into the emplacement dynamics of pyroclastic flows, *J. Geophys. Res.*, *115*, B09206, doi:10.1029/2009JB007133.
Roche, O., Y. Niño, A. Mangeney, B. Brand, N. Pollock, and G. Valentine (2013), Dynamic pore pressure variations induce substrate erosion by pyroclastic flows, *Geology*, *41*, 1107–1110, doi:10.1130/G34668.1.
Sparks, R. S. J. (1976), Grain size variations in ignimbrites and implications for the transport of pyroclastic flows, *Sedimentology*, *23*, 147–188.
Sparks, R. S. J., and L. Wilson (1976), A model for the formation of ignimbrite by gravitational column collapse, *J. Geol. Soc. London*, *132*, 441–451.
van Wyk de Vries, B., S. Self, P. W. Francis, and L. Keszthelyi (2001), A gravitational spreading origin for the Socompa debris avalanche, *J. Volcanol. Geotherm. Res.*, *105*, 225–247.
Wilson, C. J. N. (1980), The role of fluidization in the emplacement of pyroclastic flows: An experimental approach, *J. Volcanol. Geotherm. Res.*, *8*, 231–249.